Sixth International Symposium on Turbulence and Shear Flow Phenomena
Seoul, Korea, 22-24 June 2009

LARGE EDDY SIMULATION OF MIXING IN COASTAL AREAS

Federico Roman, Goran Stipcich, Vincenzo Armenio
Dipartimento di Ingegneria Civile e Ambientale,
Università degli Studi di Trieste
P.le Europa 1, 34127-Trieste, Italy
froman@units.it; goran.stipcich@phd.units.it; armenio@dica.units.it

Roberto Inghilesi, Stefano Corsini
Dipartimento Tutela delle Acque Interne e Marine,
Istituto Superiore per la Ricerca e Protezione Ambientale (ISPRA),
Via Vitaliano Brancati 48, 00144-Roma, Italy
roberto.inghilesi@ispraambiente.it; stefano.corsini@ispraambiente.it

ABSTRACT

The study of mixing in coastal area is a key issue in environmental fluid mechanics. In most applications it requires a three dimensional approach in order to take into account phenomena related to buoyancy effects and to complex geometry deriving from bathymetry, coast-line and anthropic structures. In the present paper a LES methodology is presented and discussed aimed at studying turbulent mixing in coastal areas under general forcing and geometric configuration. The strong grid anisotropy, between the horizontal length scale of kilometers and the vertical one of about 10-50 meters , is handled expressing the sub-grid stress by means of a directional eddy viscosity model. The density anomaly, due to the combination of salinity and thermal field, is treated as an active scalar in the momentum equation. Geometry is modeled using a combination of curvilinear grid and the Immersed Boundary Method (IBM). The model is applied to the investigation of two cases: the estuarine area of Tevere river; mixing in the Muggia bay under wind forcing. Results show the coastal dynamics to be strongly affected by buoyancy effects, Coriolis force and the conformation of the domain.

INTRODUCTION

The Ocean Mixed Layer (OML) is the upper layer of the ocean, adjacent to the air-sea interface, where exchange of heat, energy and momentum with the atmosphere take place. The OML is typically 10-50 meters deep in open water basins, and mixing is mainly driven by the wind shear stress, and heat exchange with air, which produces either convective or stable stratified conditions. The wind stress produces mechanical turbulence and, indirectly, additional vertical mixing through the generation of surface waves and Langmuir circulation. A review on OML is in Phillips (1977). In coastal area additional processes take place, which make modeling of mixing in the upper layer of the ocean more demanding. These regions are in general shallow and characterized by complex geometry. The shallowness makes the bottom surface layer to encroach upon the OML, hence producing a single turbulent layer extending along the whole water column. The shallowness also produces wave breaking and generation of along-shore currents. The presence of the coast-line, rapid varying bathymetry and anthropic structures introduces complexity in the flow field, making it essentially three-dimensional. In semi-closed basins (*i.e.* bays) the interaction between the wind-driven surface current and the coast-line develops a mean circulation in the vertical planes, essentially characterized by the inversion of the mean velocity field in the bottom layers of the water column with respect to the upper layer current. This creates additional shear resulting in enhanced turbulent production. Finally, buoyancy effects interacting with bathymetric gradients may favor additional circulation associated, for instance, to the downwelling of cold/salt water along the inclined bottom surface.

Traditionally, the two-dimensional shallow-water approximation has been used in coastal problems, through the use of numerical models where three-dimensional effects are parametrized by means of bulk quantities containing coefficients requiring empirical calibration. Such approach has been shown to be effective in reproducing the hydrodynamics characteristics of large scale shallow basins, where circulation in the vertical planes and buoyancy effects are negligible compared to the mean horizontal transport (Tsanis et al., 2007). In all other cases three-dimensional models must be used. Apart the numerical methods (time integration, space discretization, type of grid) these models mainly differ for the turbulence closure employed. Among them, recent models try to take advantage of Large Eddy simulation (LES) closure. The main advantage of LES compared with classical Reynolds Averaged (RANS) approach consists in the fact that the largest scales of the motion, which in a shallow-water three-dimensional basin are strongly anisotropic, are directly resolved through a three-dimensional time-dependent simulation, whereas the sub-grid scales (SGS) are parametrized through a closure model. Due to the geometric and physical complexities arising in coastal processes, a LES simulation is expected to give more accurate results compared to a RANS-like numerical model which generally uses turbulence models derived from industrial applications (mostly the aerodynamic field) and calibrated on archetypal cases typically far from being representative of coastal applications. The aim of the present research is to develop an *ad-hoc* three-dimensional LES model suited for coastal applications, thus able to take into account the physics and geometric complexities usually encountered in real-case applications. The model (LES-COAST) was developed in cooperation with the Department of Protection of Internal and Marine Waters of the Italian Agency for the Protection of the Environment (ISPRA). A description of the model is given below together with a dis-

cussion on the application to two different representative cases.

THE MATHEMATICAL MODEL

In coastal flows, often three-dimensional phenomena as *upwelling* and *downwelling* play a primary role, due to combination of the forcing terms of sea currents, wind action over the surface, buoyancy effects related to density anomalies, and Coriolis force. However, a three-dimensional coastal basin has *two* characteristic length-scales: the horizontal one (x and z axis, also denoted as 1 and 3 in the present paper) is of order of kilometers, while the vertical one (y axis, also denoted as 2) is of the order of 10-100 meters. This introduces problems in turbulence modeling as well as in numerical integration of the governing equations.

Moreover, coastal hydrodynamics is often characterized by complex geometry, mainly due to variation in bathymetry and coast-line, and to the presence of anthropic structures such as moles, jetties and wave breakers. In order to deal with geometric complexity, still retaining the accuracy and simplicity of structured-grid solvers, we use the IBM technique recently developed by Roman et al. (2008). This techniques merges the advantages of the curvilinear formulation of the Navier-Stokes equations with those of the IBM techniques.

We apply the Navier-Stokes equations under the Boussinesq approximations. In coastal applications, the density anomaly, due to salinity and temperature gradients, is small with respect to the bulk density of the water. Thus the density variations can be neglected in the governing equations, but in the gravity term present in the vertical momentum equation. When using LES methodology the variables are filtered through application of a low-pass filter and a SGS contribution appears. The filtered Boussinesq form of the Navier-Stokes equations, in Cartesian form reads as:

$$\frac{\partial \overline{u}_j}{\partial x_j} = 0 \tag{1}$$

$$\frac{\partial \overline{u}_i}{\partial t}+\frac{\partial \overline{u}_j \overline{u}_i}{\partial x_j} = -\frac{1}{\rho_0}\frac{\partial \overline{p}}{\partial x_i}+\nu\frac{\partial^2 \overline{u}_i}{\partial x_j \partial x_j}+2\Omega_i \times \overline{u_i}-\frac{\overline{\rho}}{\rho_0}g_i-\frac{\partial \tau_{ij}}{\partial x_j} \tag{2}$$

$$\frac{\partial \overline{S}}{\partial t}+\frac{\partial \overline{u}_j \overline{S}}{\partial x_j} = k_S\frac{\partial^2 \overline{S}}{\partial x_j \partial x_j}-\frac{\partial \lambda_j^S}{\partial x_j} \tag{3}$$

$$\frac{\partial \overline{T}}{\partial t}+\frac{\partial \overline{u}_j \overline{T}}{\partial x_j} = k_T\frac{\partial^2 \overline{T}}{\partial x_j \partial x_j}-\frac{\partial \lambda_j^T}{\partial x_j} \tag{4}$$

which are the continuity, the momentum and the conservation equation of salinity and the energy equation written for the temperature. The symbol "$\overline{\cdot}$" represents the filtering operation, u_i is the velocity component in i–direction, x_i is the i–direction space coordinate, t is time, p is kinematic pressure (pressure divided by reference density ρ_0) S is salinity and T is temperature. The term ν is the kinematic viscosity, Ω_i is the i–component of the rotation vector, g is the gravity vector. The values k_S and k_T in Eqs.(3,4) are the molecular diffusivities of salinity and temperature. The terms τ_{ij}, λ_j^S and λ_j^T are respectively the SGS momentum, salinity and temperature fluxes. The density ρ is related to temperature and salinity through the state equation:

$$\rho = \rho_0[1-\alpha(T-T_0)+\beta(S-S_0)] \tag{5}$$

where ρ_0 is the density at a temperature T_0 and salinity S_0 and α and β are the thermic and salinity expansion coefficient respectively.

As regards SGS modeling, the dynamic model may be not suited for our application for two main reasons: first, literature studies show that the dynamic model is not suited for high Reynolds number, large-scale flows (Bou-Zeid et al., 2005), due to the lack of scale invariance between the SGS and the subtest stresses; second, the explicit filtering required by the dynamic procedure may be problematic when working with IBM. Thus we move back to the Smagorinsky model. However, the discretization of a 3D coastal basin commonly leads to $pancake-like$ anisotropic cells, with an aspect ratio of $10-100:1$, and this can give rise to modeling problems in LES when reproducing the sub-grid stress (SGS). For unequal-sided cells the Deardroff equivalent length scale $\Delta_{eq} = (\Delta_1\Delta_2\Delta_3)^{1/3}$ is commonly used, where Δ_i $(i = 1,2,3)$ is the cell side in the $i-$direction. This is a good choice for weakly anisotropic grid, but for $cigar-like$ or $sheet-like$ cells, as in our cases, it determines anisotropic filtering of a turbulent field which is essentially isotropic. Consequently, inaccuracies may occur in the evaluation of turbulent statistics (Kaltenbach, 1997).

Scotti et al. (1993) investigated the performance of the Smagorinsky model with different length-scales in the case of inhomogeneous flow. They defined a single length-scale obtaining a model which is close to that for isotropic case. Successively Zahrai et al. (1995) proposed a model with different length-scales. Our strategy consists to move back to the Smagorinsky model with different length-scales, a solution which is well suited for highly anisotropic filtering cells, being the use of a single characteristic length-scale no longer appropriate (Sagaut, 1998). This model works well in conjunction with wall layer models and immersed boundaries. The SGS stress is expressed as the sum of a scale similar component and an eddy viscosity component as:

$$\tau_{SGS,ij} = -2\nu_t \overline{S}_{ij}+\overline{\overline{u}_i \overline{u}_j}-\overline{\overline{u}}_i\,\overline{\overline{u}}_j \tag{6}$$

where $\overline{S}_{ij}$ is the resolved strain rate tensor

$$\overline{S}_{ij} = \frac{1}{2}\left(\frac{\partial \overline{u}_i}{\partial x_j}+\frac{\partial \overline{u}_j}{\partial x_i}\right) \tag{7}$$

ν_t is the eddy viscosity.

The scale similar part in Eq.(6) accounts for local backscatter and anisotropy, whereas the Smagorinsky part of the model supplies most of SGS dissipation. The original model is isotropic, based on the assumption that the small scales tend to isotropy, which is not true for large scale coastal dynamics, where the SGS part of the spectrum contains a wide range of anisotropic structures. The eddy viscosity is evaluated as the product of a length-scale $C\Delta$, proportional to the grid size, and a velocity scale $C\Delta|\overline{S}|$, where C is a constant and $|\overline{S}|$ is the contraction of the strain rate tensor. The requirement of having a single length-scale in an anisotropic grid can be overcome by considering different eddy viscosities for the horizontal and for the vertical direction respectively. This is a standard technique in large-scale ocean models. Two eddy viscosities $\nu_{t,h}$ and $\nu_{t,v}$ are commonly used in geophysical fluid dynamics (Pedlosky, 1987), with h and v denoting the horizontal and the vertical component respectively. The diffusive term for the Navier-Stokes equations reads as:

$$F_i = \frac{\partial}{\partial x_1}\nu_h\frac{\partial \overline{u}_i}{\partial x_1}+\frac{\partial}{\partial x_2}\nu_h\frac{\partial \overline{u}_i}{\partial x_2}+\frac{\partial}{\partial x_3}\nu_v\frac{\partial \overline{u}_i}{\partial x_3} \tag{8}$$

where $\nu_h = \nu+\nu_{t,h}$ and $\nu_v = \nu+\nu_{t,v}$. Although widely in use, this formulation is not mathematically consistent since

it takes into account only deformation and not rotation in the definition of the stress. The assumption of linear proportionality with $\overline{S}_{ij}$ is not true if we introduce directional eddy viscosities. A correct tensorial analysis requires three different eddy viscosities (Kamenkovich, 1977; Mills, 1994): $\nu_{11} = \nu_{13} = \nu_{33}$, $\nu_{12} = \nu_{23}$, and ν_{22}, with $\nu_{ij} = \nu_{ji}$. Using a Smagorinsky model we have the relations

$$\nu_{11} = (CL_h)^2|\overline{S}_h| \tag{9}$$

$$\nu_{12} = (CL_v)^2|\overline{S}_v| \tag{10}$$

$$\nu_{22} = (CL_v)^2|\overline{S}_r| \tag{11}$$

where L_h and L_v are proper length-scales for horizontal and vertical direction respectively, while the strain rate tensor is decomposed as

$$|\overline{S}_h| = \sqrt{2(\overline{S}_{11}^2 + \overline{S}_{33}^2 + 2\overline{S}_{13}^2)} \tag{12}$$

$$|\overline{S}_v| = \sqrt{4(\overline{S}_{12}^2 + \overline{S}_{23}^2)} \tag{13}$$

$$|\overline{S}_r| = \sqrt{2\overline{S}_{22}^2} \tag{14}$$

If we consider $\nu_{11} = \nu_{t,h}$ and $\nu_{12} = \nu_{t,v}$ the diffusive term for the horizontal plane can be written as in Eq.(8). While for the vertical direction 2 we have

$$F_2 = \frac{\partial}{\partial x_1}\nu_v\frac{\partial \overline{u}_2}{\partial x_1} + \frac{\partial}{\partial x_2}\nu_v\frac{\partial \overline{u}_2}{\partial x_2} + \frac{\partial}{\partial x_3}\nu_r\frac{\partial \overline{u}_2}{\partial x_3} \tag{15}$$

where $\nu_r = \nu + \nu_{t,r}$ and $\nu_{t,r} = \nu_{11} - 2\nu_{12} + 2\nu_{22}$. The coefficients of the model need calibration and this is still an open issue for lacking of proper test cases.

The algorithm integrates the equations using the curvilinear-grid, fractional-step method of Zang et al. (1994). All terms are treated explicitly through second-order Adams-Bashfort technique except the diagonal diffusive ones, which are treated implicitly. Spatial derivatives are treated using centered second-order finite differences, but the advective terms that are discretized using a 3rd-order accurate QUICK scheme. The pressure equation is solved using a line-SOR algorithm, with line solution in the vertical direction and point iteration in the horizontal directions, in conjunction with a Multigrid technique to speed up the convergence.

The high value of Re and the presence of roughness in this kind of applications makes unfeasible the direct solution of the near wall layer, thus the problem is approached parameterizing the near-wall layer through the use of a model. We impose a wall layer model as follows: to find the velocity at an interface node IB we consider its normal to the immersed boundary, then we interpolate the resolved velocity field onto a fictitious node PP lying on this normal line. If the logarithmic law is assumed to hold on both these nodes IB and PP, one obtains the following relation to determine the velocity at IB

$$u_{tan,IB} = u_{tan,PP} - \frac{1}{k}\sqrt{\frac{\tau_w}{\rho_0}}\log\frac{d_{PP}}{d_{IB}} \tag{16}$$

with u_{tan} the tangential velocity, k the von Karman constant, τ_w the wall stress, ρ_0 the density, and d the distance from the immersed boundary. To model the eddy viscosity part of the SGS stress we use a Smagorinsky model.

Close to the wall the eddy viscosity is computed using a length-scale and a velocity-scale characteristic of the non-resolved structures, and using the equilibrium assumption they can be related to the resolved motion through the grid size and the strain rate tensor. The presence of an immersed boundary can however yield an incorrect representation of these scales. Hence, at the IB interface we use the logarithmic law to derive the following relationship:

$$\nu_{t,IB} = cku_\tau d_{IB} \tag{17}$$

which relates the length-scale and the velocity-scale to the presence of the immersed boundary; here u_τ is the friction velocity ($u_\tau = \sqrt{\tau_w/\rho_0}$). The model is described in details in Roman et al. (2009).

The SGS fluxes of the scalar quantities are parametrized in a very simple way, using a model similar to that of momentum transport and evaluating the eddy diffusivities as $Pr_{sgs} = Sc_{sgs} = 0.5$, with Pr_{sgs} and Sc_{sgs} the Prandtl number ($Pr_{sgs} = \nu_t/k_{t,T}$ with $k_{t,T}$ the thermal eddy diffusivity) and Schmidt number ($Sc_{sgs} = \nu_t/k_{t,S}$ with $k_{t,S}$ the salinity eddy diffusivity) respectively. This value has been found in literature to hold for a wide range of conditions of stratification, from convective conditions to weakly stratified ones. In strongly stratified cases a different closure should be employed for the SGS scalar fluxes.

Finally, the effect of the wind over the free surface is modeled through direct application of the friction velocity u_τ associated to the wind stress, obtained as

$$u_\tau \;=\; U_{10}\sqrt{C_{10}\frac{\rho_a}{\rho_0}} \tag{18}$$

where U_{10} is a fixed value of wind speed at $10\,m$ over the surface, ρ_a is the air density, and the parameter C_{10} is calculated as (Wu, 1982):

$$C_{10} \;=\; (0.8 + 0.065\,U_{10})10^{-3} \tag{19}$$

The wind stress is not constant in space, rather it has a certain statistical distribution around a mean value, so that the final expression for the friction velocity is

$$u_{\tau def} \;=\; u_\tau G(0\,;\,q) \tag{20}$$

where G is a random Gauss function with zero mean value and variance q.

APPLICATIONS: RESULTS AND DISCUSSION

The model has been used to investigate two different coastal areas. The first application regards the mixing effects due to the incoming flow of fresh water from Tevere river into the Thirrenian sea, the second one regards the analysis of mixing and circulation within a semi-closed bay in the Trieste harbor area.

Case 1: Tevere's estuarine flow

The area of interest is the estuary of Tevere river, near Rome, in Italy, whose sketch is reported in Fig.(1). The domain covers an area of $5\,km \times 6\,km$ in the horizontal plane, while on the vertical one the maximum depth is of about $30\,m$. We use 385×385 grid points along the horizontal directions x and z, and 33 grid points along the vertical direction y. This gives rise to cells of about $10\,m \times 10\,m \times 0.4\,m$. Fig.(2a) shows the free surface grid plane, and Fig.(2b) is the grid bottom surface constructed from bathymetric data. The coast-line and the upper part of the bathymetry are treated using the IBM.

The boundary conditions are chosen in the following way. On the sea bottom and on solid walls we use a wall function.

On the vertical boundary SE-SO we consider the presence of a along-shore sea current of $0.02\,m/s$, which is a typical value for the region examined. On the NE-SE boundary we consider an inflow condition corresponding to the Tevere river. This inflow was created by a pre-simulation of a turbulent channel flow with the same geometry and flow-rate of the river. The average velocity is about $0.3\,m/s$, and the flow rate is about $300\,m^3/s$, typical winter time values for Tevere river. The channel flow is pre-simulated considering the presence of the Coriolis force. On the sea surface we consider a free-slip condition, while on the remaining, open, boundaries an Orlanski condition is enforced.

The incoming flow from the river has the density of fresh water, which is smaller than the salt water's density of the receiving basin. Stratification is only due to this salinity difference. The analysis of the horizontal length-scales and of the typical velocity scales shows that the Coriolis force cannot be neglected.

Figure 3a shows the contour plot of the horizontal velocity component u on an horizontal plane. Once in the sea, the river flow tends to deviate north, driven by the southern sea current and by the Coriolis force. The main current merges into the sea far from the coast-line, and a large recirculation area is trapped in between. The Coriolis force produces an asymmetric profile with a larger velocity near the northern bank of the river's mouth. Fig.(3b) shows a plot of the vertical velocity v on an horizontal plane. The contour legend shows that the vertical velocity is one order of magnitude smaller than the horizontal one, as expected for these kinds of flows. The two figures refer to an horizontal layer just below the sea surface. The same overall behavior is observed at different depths. Figures 4a,b show the horizontal and vertical components of eddy viscosity ν_t, $2\,m$ below the surface. The vertical eddy viscosity is one order of magnitude smaller than the horizontal one and they are large within the current showing large turbulent mixing in this region.

In Figs.5a,b density contours at different depths are shown. Because of the buoyancy, the light fresh water coming from the river tends to rise over the salt water and to spread in the horizontal directions. Then the fresh water is transported by the mean current and turns north without reaching the coast far from the river's mouth.

The results show that the model is able to catch the expected behavior for sea coastal area. A qualitative comparison is shown in Fig.(6) between velocity vectors obtained in the simulation and a satellite image highlighting the main river stream.

Case 2: Trieste harbor area

The aim of this application is to study the three-dimensional circulation in the Muggia bay, where the Trieste harbor is located (Italy), under a specified forcing wind condition. Fig.(7) reports a satellite image of the area. The bay is bounded by the coast line on the north, east and south sides, while on the west side a system of breakwater separates the bay from the rest of the gulf. The dimensions of the domain are $5\,km \times 4\,km$ in the horizontal plane, while the maximum depth is of $21\,m$. The discretization involves, on the horizontal plane, 285×257 grid points along x and z axis, and 25 grid points along the y axis. The resulting cells are *sheet*-shaped, with typical dimensions of $10\,m \times 10\,m \times 0.5\,m$. Fig.(8a) shows the horizontal perimeter of the grid, and in Fig.(8b) the shape of the bottom reproducing the actual bathymetry is depicted. The coast line and the upper part of the bathymetry are treated using the IBM.

The boundary conditions are set in the following way: on the solid walls we use a wall function, on the sea surface a south-west forcing wind is imposed with intensity of $U_{10} = 4\,m/s$. This is a typical value for wind in this geographical area. On the remaining, open, boundaries an Orlanski condition is enforced. As in the previous case the Coriolis effects are taken into account.

Figure 9a shows the contour plot of the horizontal velocity component u $2\,m$ below the surface. The order of magnitude is of about $0.1\,m/s$, which is a mean value for the Trieste gulf's currents. Intense currents in the bay are observed in open areas, that is, far from the coast line and breakwater, where wind fetch has higher values. The main inward current is found in the Southern Canal. Less intense fluxes are observed between the different breakwaters, in the surface and bottom layers respectively. We noted the presence of two main types of recirculation motions. The first one is generated by the surface leading current which, colliding with the coast-line on the N-E side, deviates into deeper layers and flows in the opposite direction. The inverted bottom-layers circulation has an intensity of an order of magnitude smaller than the superficial one, which is typical for this geographical area. Figure 9b shows the contour plot of u, $6\,m$ below the surface. It can be noticed the small value of the mean velocity (compared to the surface current) and the presence of the bottom recirculation currents. The second ones are $down-$ and $up-welling$ phenomena due to the surface wind action, which produces small scale eddies between the surface and the bottom. These are due to the presence of obstacles in quite deep water, such as the area of the commercial port, or near the jetties. The $down$ and $up-welling$ structures can be noted as they have opposite flow directions.

Figures 10a,10b show the horizontal component of eddy viscosity ν_t at the surface level and $3\,m$ below the free surface. In the free-surface layer the highest turbulent dissipation is observed to occur close to the presence of the physical obstacles such as break- water, coast-line, jetties. In the deep layers turbulent dissipation denotes the presence of middle-high currents and recirculations.

Overall the analysis shows that under the wind forcing herein investigated a quite poor exchange of water in the bay is observed, because of its own conformation and the presence of break waters. Different wind conditions are at the present under analysis, in order to have a more complete description of the bay's water dynamics.

REFERENCES

Bou-Zeid, E., Meneveau, C., Parlange, M.B., 2005, *Physics of Fluids*, vol. 17.

Kaltenbach, H. J. 1997, "Cell aspect ratio dependence of anisotropy measures for resolved and subgrid scale stresses", *J. Comput. Phys.* **136**, 399–410.

Kamenkovich, V. M., 1977, "Fundamentals of ocean dynamics", Elsevier.

Mills, J., 1994, "On transversely isotropic eddy viscosity", *J. of Physical Oceanography* **24**, 1077–1079.

Phillips, O. M., 1977, "The dynamics of the Upper Ocean", 2nd Edition, Cambridge University Press.

Pedlosky, J., 1987, "Geophysical fluid dynamics", Springer.

Roman, F., Napoli, E., Milici, B., Armenio, V., 2008, "An improved Immersed Boundary Method for curvilinear grids", *Computers & Fluids*, in press.

Roman, F., Fröhlich, J., Armenio, V., 2009, "A wall

model for Large Eddy Simulation with an Immersed Boundary Method" *Academy / EUROMECH / ERCOFTAC Colloquium, Immersed Boundary Methods: Current Status and Future Research Directions, Amsterdam, the Netherlands, June 2009 (Accepted)*

Sagaut, P., 1998, "Large Eddy Simulations for incompressible flows, an introduction", Springer Verlag.

Scotti, A., Meneveau, C., Lilly, D.K., 1993, "Generalized Smagorinsky model for anisotropic grids", *Phys. Fluids* **5**(9), 2306–2308.

Tsanis, I.K., Wu, J., Shen H., Valeo C., 2007, "Environmental Hydraulics", Developments in Water Sciences, Vol. 56, Elsevier.

Wu, J., 1982, "Wind-stress coefficients over sea surface from breeze to hurricane", J. Geophys. Research., C87:9704-9706.

Zahrai, S., Bark, F.H., Karlsson, R.I., 1995, "On anisotropic subgrid modeling", *Eur. J. Mech. B/Fluids* **14**(4), 459-486.

Zang, Y., Street, R.L., Koseff, J., 1994, "A non-staggered grid fractional step method for time-dependent incompressible Navier-Stokes equations in curvilinear coordinates", *J. Comput. Phys.* **114**, 18-33.

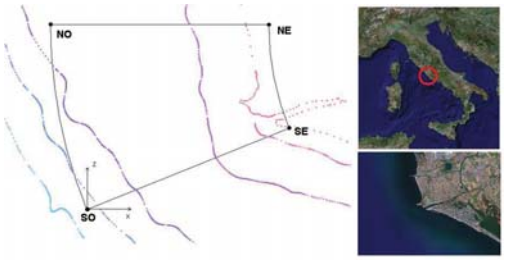

Figure 1: Case 1 Bathymetry, grid edges and physical domain for Tevere river area.

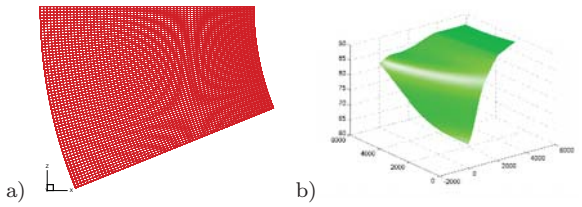

Figure 2: Case 1 a) Horizontal plane for a coarse grid. b) Bottom of the grid from bathymetry.

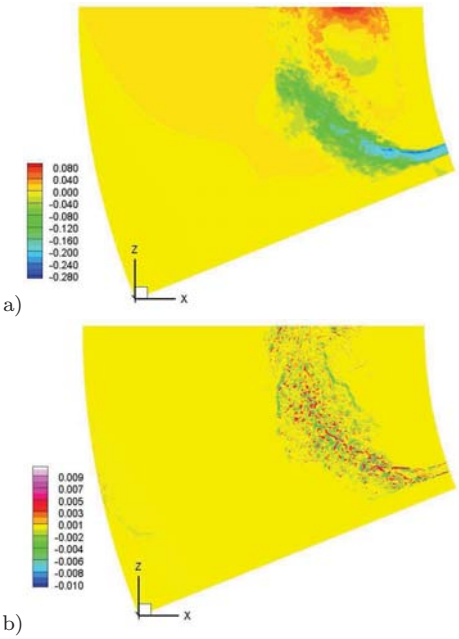

Figure 3: Case 1 a) Contour of the horizontal velocity component u on an horizontal plane at $1\,m$ below the surface. b) Contour of the vertical velocity component v on an horizontal plane at $1\,m$ below the surface.

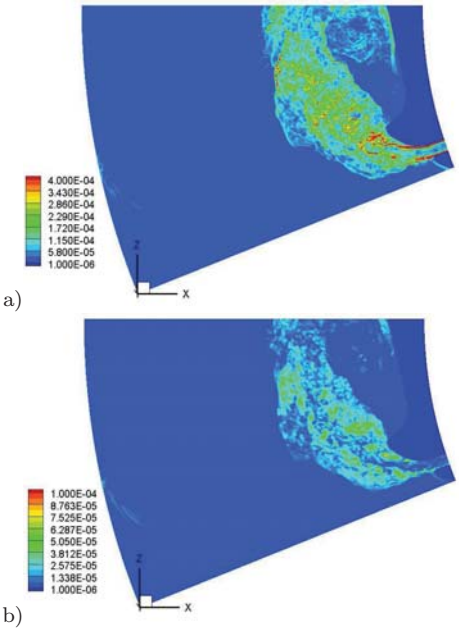

Figure 4: Case 1 Plot of the eddy viscosity ν_t at $1\,m$ below the surface: a) horizontal component, b) vertical component.

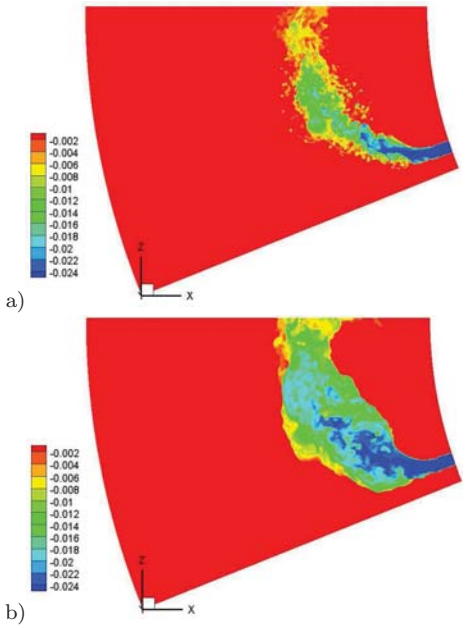

Figure 5: Case 1 a) Ratio ρ'/ρ_0 at $5\,m$ from the sea surface. b) Ratio ρ'/ρ at the sea surface.

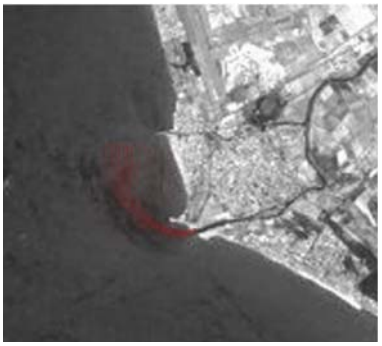

Figure 6: Case 1 A satellite image of Tevere's mouth.

Figure 7: Case 2 Physical domain of the Trieste harbor.

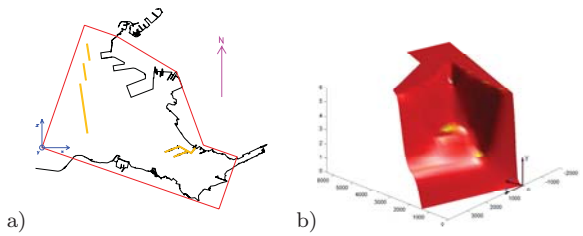

Figure 8: Case 2 a) Horizontal plan of the computational grid. b) Bottom of the grid following the bathymetry.

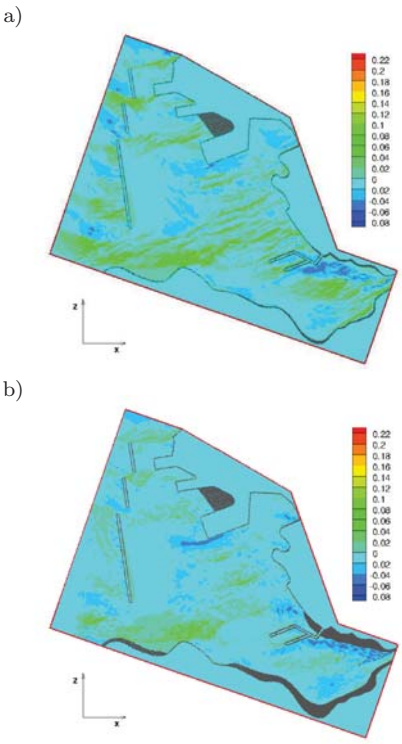

Figure 9: Case 2 a) Contour of the horizontal velocity component u on an horizontal plane, at a depth of $2\,m$ below the sea surface. b) Contour of the horizontal velocity component u on an horizontal plane, at a depth of $6\,m$ below the sea surface.

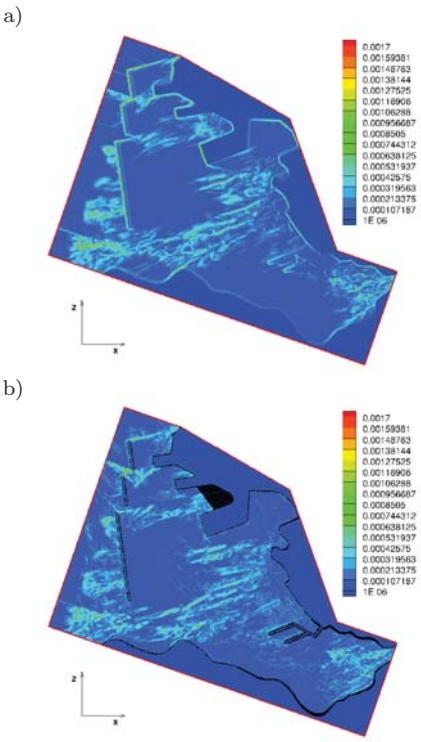

Figure 10: Case 2 a) Plot of the horizontal eddy viscosity $\nu_{t,h}$: a) surface level, b) depth of $3\,m$ below the surface.